AMERICAN SOCIETY FOR MICROBIOLOGY | mBio®

RESEARCH ARTICLE
Therapeutics and Prevention

Rescue of SARS-CoV-2 from a Single Bacterial Artificial Chromosome

Chengjin Ye,[a] Kevin Chiem,[a] Jun-Gyu Park,[a] Fatai Oladunni,[a,b] Roy Nelson Platt II,[a] Tim Anderson,[a] Fernando Almazan,[c] Juan Carlos de la Torre,[d] Luis Martinez-Sobrido[a]

[a]Texas Biomedical Research Institute, San Antonio, Texas, USA
[b]Department of Veterinary Microbiology, University of Ilorin, Ilorin, Nigeria
[c]Department of Molecular and Cell Biology, Centro Nacional de Biotecnología (CNB-CSIC), Madrid, Spain
[d]Department of Immunology and Microbiology, The Scripps Research Institute, La Jolla, California, USA

ABSTRACT Infectious coronavirus (CoV) disease 2019 (COVID-19) emerged in the city of Wuhan (China) in December 2019, causing a pandemic that has dramatically impacted public health and socioeconomic activities worldwide. A previously unknown coronavirus, severe acute respiratory syndrome CoV-2 (SARS-CoV-2), has been identified as the causative agent of COVID-19. To date, there are no U.S. Food and Drug Administration (FDA)-approved vaccines or therapeutics available for the prevention or treatment of SARS-CoV-2 infection and/or associated COVID-19 disease, which has triggered a large influx of scientific efforts to develop countermeasures to control SARS-CoV-2 spread. To contribute to these efforts, we have developed an infectious cDNA clone of the SARS-CoV-2 USA-WA1/2020 strain based on the use of a bacterial artificial chromosome (BAC). Recombinant SARS-CoV-2 (rSARS-CoV-2) was readily rescued by transfection of the BAC into Vero E6 cells. Importantly, BAC-derived rSARS-CoV-2 exhibited growth properties and plaque sizes in cultured cells comparable to those of the natural SARS-CoV-2 isolate. Likewise, rSARS-CoV-2 showed levels of replication similar to those of the natural isolate in nasal turbinates and lungs of infected golden Syrian hamsters. This is, to our knowledge, the first BAC-based reverse genetics system for the generation of infectious rSARS-CoV-2 that displays features *in vivo* similar to those of a natural viral isolate. This SARS-CoV-2 BAC-based reverse genetics will facilitate studies addressing several important questions in the biology of SARS-CoV-2, as well as the identification of antivirals and development of vaccines for the treatment of SARS-CoV-2 infection and associated COVID-19 disease.

IMPORTANCE The pandemic coronavirus (CoV) disease 2019 (COVID-19) caused by severe acute respiratory syndrome CoV-2 (SARS-CoV-2) is a major threat to global human health. To date, there are no approved prophylactics or therapeutics available for COVID-19. Reverse genetics is a powerful approach to understand factors involved in viral pathogenesis, antiviral screening, and vaccine development. In this study, we describe the feasibility of generating recombinant SARS-CoV-2 (rSARS-CoV-2) by transfection of a single bacterial artificial chromosome (BAC). Importantly, rSARS-CoV-2 possesses the same phenotype as the natural isolate *in vitro* and *in vivo*. This is the first description of a BAC-based reverse genetics system for SARS-CoV-2 and the first time that an rSARS-CoV-2 isolate has been shown to be phenotypically identical to a natural isolate in a validated animal model of SARS-CoV-2 infection. The BAC-based reverse genetics approach will facilitate the study of SARS-CoV-2 and the development of prophylactics and therapeutics for the treatment of COVID-19.

KEYWORDS BAC, COVID-19, SARS-CoV-2, coronavirus, hamsters, recombinant virus, reverse genetics

Citation Ye C, Chiem K, Park J-G, Oladunni F, Platt RN, II, Anderson T, Almazan F, de la Torre JC, Martinez-Sobrido L. 2020. Rescue of SARS-CoV-2 from a single bacterial artificial chromosome. mBio 11:e02168-20. https://doi.org/10.1128/mBio.02168-20.

Editor Anne Moscona, Columbia University Medical College

Address correspondence to Luis Martinez-Sobrido, lmartinez@txbiomed.org.

Received 1 August 2020
Accepted 8 September 2020
Published 25 September 2020

In December 2019, a previously unknown coronavirus (CoV) was isolated in Wuhan (China) from a patient with respiratory disease who had possible contact with wild animals (1–3). Since then, severe acute respiratory syndrome CoV-2 (SARS-CoV-2), the ethological agent responsible for CoV disease 2019 (COVID-19), has been detected in 216 countries, areas, or territories, and it has been responsible for over 11,125,245 human cases and 528,204 deaths (https://www.who.int/emergencies/diseases/novel-coronavirus-2019). The unprecedented human health and socioeconomic impact of COVID-19 rivals only that of the "Spanish flu" pandemic, which occurred almost 100 years ago (4–8). To date, there are no U.S. Food and Drug Administration (FDA)-approved prophylactics (vaccines) or specific therapeutics (antivirals) available for the prevention and treatment, respectively, of SARS-CoV-2-associated COVID-19 disease.

CoVs are enveloped, single-stranded, positive-sense RNA viruses belonging to the *Nidovirales* order and responsible for causing seasonal mild respiratory illness in humans (e.g., 229E, NL63, OC43, HKU1). However, two previous CoVs have been associated with severe illnesses and resulted in significant morbidity and mortality in humans. These were severe acute respiratory syndrome CoV (SARS-CoV) in 2002 and Middle East respiratory syndrome CoV (MERS-CoV) in 2012 (9). Like that of SARS-CoV, the SARS-CoV-2 genome is approximately 30,000 bases in length. Nonetheless, a feature of SARS-CoV-2 that is unique among known betacoronaviruses is the presence of a furin cleavage site in the viral spike (S) glycoprotein, a characteristic known to increase pathogenicity and transmissibility in other viruses (10).

The ability of generating recombinant viruses using reverse genetics approaches represents a powerful tool to answer important questions in the biology of viral infections. It will help us to understand the mechanisms of viral infection, transmission, and pathogenesis, as well as to identify viral and host factors and interactions that control viral cell entry, replication, assembly, and budding. In addition, reverse genetics facilitates the generation of recombinant viruses expressing reporter genes for their use in cell-based screening assays or *in vivo* models of infection for the rapid and easy identification of prophylactic and therapeutic approaches for the treatment of viral infections, as well as to generate attenuated forms of viruses for their implementation as safe, immunogenic, and protective live attenuated vaccines (LAVs).

DNA plasmids that replicate in *Escherichia coli* have previously been used for the cloning of many viral genomes and generation of reverse genetics systems. However, assembly of full-length cDNAs of viruses with a large viral genome in *E. coli* is very challenging technically due to the toxicity, instability, or both of sequences within the viral genome. Two recent papers have described the ability to assemble the full-length genome of SARS-CoV-2 by *in vitro* ligation (11) or homologous recombination in *Saccharomyces cerevisiae* (12) to overcome this problem. However, both approaches rely on production of the full-length viral genome RNA by *in vitro* transcription, a process that poses technical difficulties. Bacterial artificial chromosomes (BACs), which are maintained as a single copy in *E. coli*, have previously been described to establish a reverse genetics system for large RNA viruses, including other CoVs (13–15). To date, the use of a single BAC for the rescue of recombinant SARS-CoV-2 (rSARS-CoV-2) has not yet been described. In this article, we describe the development of a BAC-based reverse genetics system for the recovery of rSARS-CoV-2 from transfected Vero E6 cells. Importantly, our results show that rSARS-CoV-2 and the natural SARS-CoV-2 isolate have similar levels of fitness in cultured cells and replicate to similar levels in a validated golden Syrian hamster model of SARS-CoV-2 infection and associated COVID-19 disease. This is the first description of a reverse genetics approach for the rescue of rSARS-CoV-2 based on the use of a single BAC. This approach will facilitate studies on the biology of SARS-CoV-2, as well as the identification and characterization of antivirals and the development of LAVs for the control of SARS-CoV-2 infection and associated COVID-19 disease.

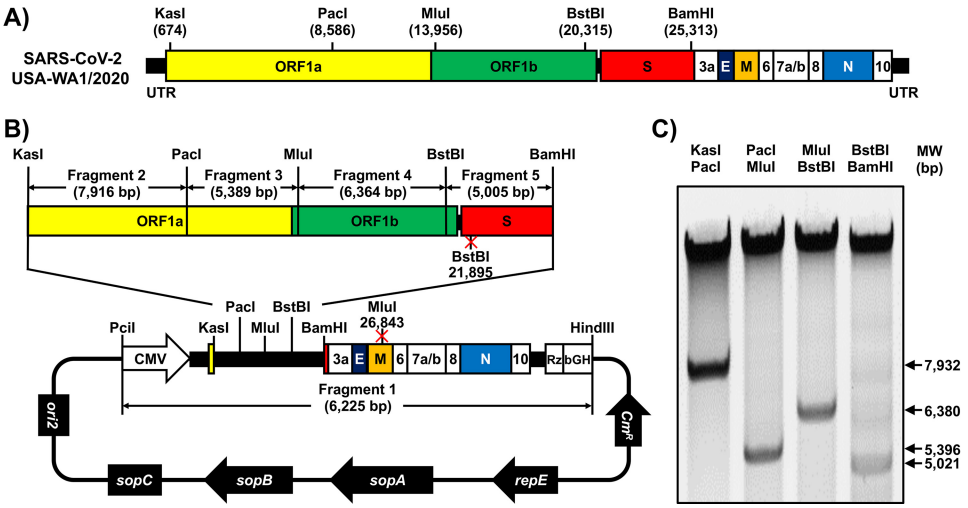

FIG 1 Assembly of the SARS-CoV-2 genome into a BAC. (A) Schematic representation of the SARS-CoV-2 genome. The indicated restriction sites were used for cloning the entire viral genome (29,903 nucleotides) of SARS-CoV-2, USA-WA1/2020 strain, into the pBeloBAC11 plasmid. The open reading frames of the viral structural 1a, 1b, spike (S), envelop (E), matrix (M), and nucleocapsid (N) proteins and the accessory (3a, 6, 7a, 7b, 8, and 10) proteins are also indicated. UTR, untranslated regions. Length is not to scale. (B and C) Assembly of the viral genome. (B) The full-length infectious cDNA clone was assembled by sequentially cloning chemically synthesized fragments 1 to 5, which covers the entire viral genome, into the pBeloBAC11 plasmid by using the indicated restriction sites under the control of the cytomegalovirus (CMV) promoter; the clone was flanked at the 3′ end by the hepatitis delta virus (HDV) ribozyme (Rz) and the bovine growth hormone (bGH) termination and polyadenylation sequences. The length of each of the chemically synthesized viral fragments is indicated. Ori2 indicates the origin of the replication of BAC. *sopA*, *sopB*, and *sopC* are the elements to ensure that each bacterial cell gets a copy of the BAC. Cm^R indicates chloramphenicol resistance. (C) After assembly, the BAC clone harboring the entire viral genome was digested with the indicated restriction enzymes (top), and DNA products were analyzed in a 0.5% agarose gel.

RESULTS

Assembly of the SARS-CoV-2 genome in the BAC. We used a BAC-based approach, similar to the one that we previously described for Zika virus (16–21), to assemble an infectious clone of SARS-CoV-2 based on the USA-WA1/2020 strain (Fig. 1A). We selected this SARS-CoV-2 strain because it was isolated from an oropharyngeal swab from a patient with respiratory illness in Snohomish County, Washington state, USA. The viral sequence was deposited in PubMed, and the virus isolate is available from BEI Resources.

We chemically synthesized the entire viral genome in 5 fragments, which were assembled in the pBeloBAC plasmid using unique restriction enzymes and standard molecular biology approaches (Fig. 1B). After assembly of the 5 fragments, the BAC containing the entire viral genome was analyzed by restriction enzyme analysis (Fig. 1C). To facilitate the assembly of the viral genome and incorporate genetic tags to distinguish the rSARS-CoV-2 clone from the natural isolate, we introduced two silent mutations in the viral genes for S (21,895 nucleotides [nt]) and matrix (M) (26,843 nt) that removed BstBI and MluI restriction sites, respectively (Fig. 1B).

Rescue of rSARS-CoV-2. To recover rSARS-CoV-2, we used an experimental approach similar to one that we previously described for mammarenaviruses (22, 25) (Fig. 2A). Vero E6 cells were transfected with the SARS-CoV-2 BAC or an empty BAC as an internal control and were monitored for the presence of cytopathic effect (CPE), which was evident at 72 h posttransfection (Fig. 2B). Production of infectious virus (designated passage 0 [P0]) by transfected cells was at 3.4×10^5 PFU/ml (Fig. 2C). Recovery of rSARS-CoV-2 was confirmed by detection of viral antigen in fresh Vero E6 cells infected with tissue culture supernatants collected from SARS-CoV-2 BAC-transfected Vero E6 cells, but not from empty BAC-transfected Vero E6 cells, by immunofluorescence using a monoclonal antibody against the nucleocapsid (N) protein of SARS-CoV that cross-reacts with SARS-CoV-2 N (Fig. 2D).

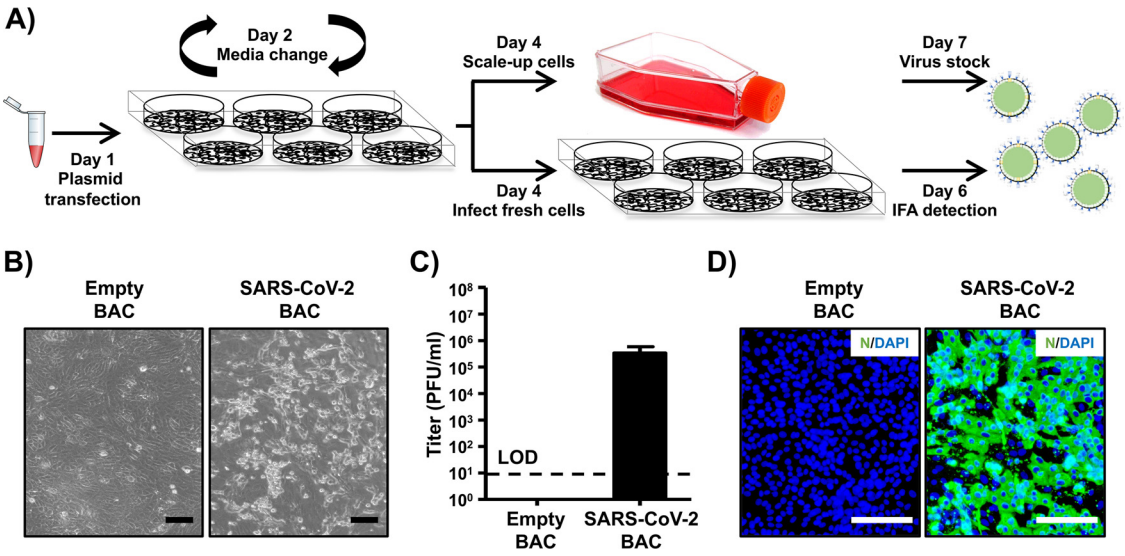

FIG 2 Rescue of rSARS-CoV-2. (A) Schematic representation of the approach followed to rescue rSARS-CoV-2. Vero E6 cells were transiently transfected with the SARS-CoV-2 BAC at day 1. After 24 h, transfection medium was changed to postinfection medium. At day 4, cells were split into T75 flasks and the tissue culture supernatant was used to infect fresh Vero E6 cells. At 48 h postinfection, Vero E6 cells were fixed for detection of rSARS-CoV-2 by immunofluorescence, and the tissue culture supernatant of the scaled-up Vero E6 cells was collected at 72 h. As an internal control for this experiment, Vero E6 cells were transfected with the empty BAC. (B) CPE. Images of empty or SARS-CoV-2 BAC-transfected Vero E6 cells at 72 h posttransfection are shown. Scale bars, 100 μm. (C) Viral titers. Tissue culture supernatant from mock-infected (empty BAC) or transfected Vero E6 cells in T75 flasks was collected and titrated by immunofluorescence. Data are presented as means ± SDs. LOD, limit of detection. (D) IFA. Vero E6 cells infected with the tissue culture supernatants from transfected Vero E6 cells were fixed at 48 h postinfection, and viral detection was carried out by using a SARS-CoV cross-reactive monoclonal antibody (1C7) against the N protein (green). Cellular nuclei were stained by 4′,6-diamidino-2-phenylindole (DAPI; blue). Scale bars, 100 μm.

Characterization of rSARS-CoV-2 *in vitro*. We first confirmed the genetic identity of the rescued rSARS-CoV-2 clone. To that end, we used total RNA isolated from rSARS-CoV-2- and SARS-CoV-2-infected Vero E6 cells to amplify by real-time PCR (RT-PCR) a region in the M gene (nt 26488 to 27784), from which an MluI restriction site was removed from the rSARS-CoV-2 cDNA via a silent mutation (Fig. 1B). As expected, the RT-PCR product from SARS-CoV-2-infected cells digested with MluI yielded two fragments with sizes of 351 and 946 bp (Fig. 3A, bottom). In contrast, the RT-PCR product from rSARS-CoV-2-infected cells was not digested with MluI (Fig. 3A, bottom). We confirmed the mutation introduced into the MluI restriction site in the rSARS-CoV-2 strain by Sanger sequencing (Fig. 3B).

To further characterize the genetic identity of rSARS-CoV-2, we used next-generation sequencing (NGS) to determine the complete genome sequence of the natural SARS-CoV-2 isolate from BEI Resources and the rescued rSARS-CoV-2 RNA, as well as the BAC plasmid used to rescue rSARS-CoV-2. We examined 4.95 million, 5.79 million, and 5.44 million reads for the natural virus isolated, BAC plasmid, and rescued rSARS-CoV-2 RNA, resulting in coverages of 978×, 15,296×, and 1,944× per sample, respectively. Introduced variants were not present in the SARS-CoV-2 RNA but were effectively fixed in the BAC plasmid and rSARS-CoV-2. We confirmed the presence of the genetic markers at positions 21895 (S) and 26843 (M) in both the BAC plasmid and rSARS-CoV-2 (allele frequencies, >99.9%) (Fig. 3C, middle and bottom).

Next, we compared rSARS-CoV-2 and the natural isolate of SARS-CoV-2 with respect to their growth properties in Vero E6 cells. Both rSARS-CoV-2 and SARS-CoV-2 made uniform plaques of similar sizes (Fig. 3D). Likewise, both rSARS-CoV-2 and SARS-CoV-2 exhibited similar growth kinetics and peak titers (Fig. 3E). These results confirmed the genetic identity of rSARS-CoV-2 and its ability to replicate to the same extent as the SARS-CoV-2 natural isolate in Vero E6 cells.

Pathogenicity of rSARS-CoV-2 *in vivo*. Golden Syrian hamsters (*Mesocricetus auratus*) have been shown to be a good rodent animal model for investigating the

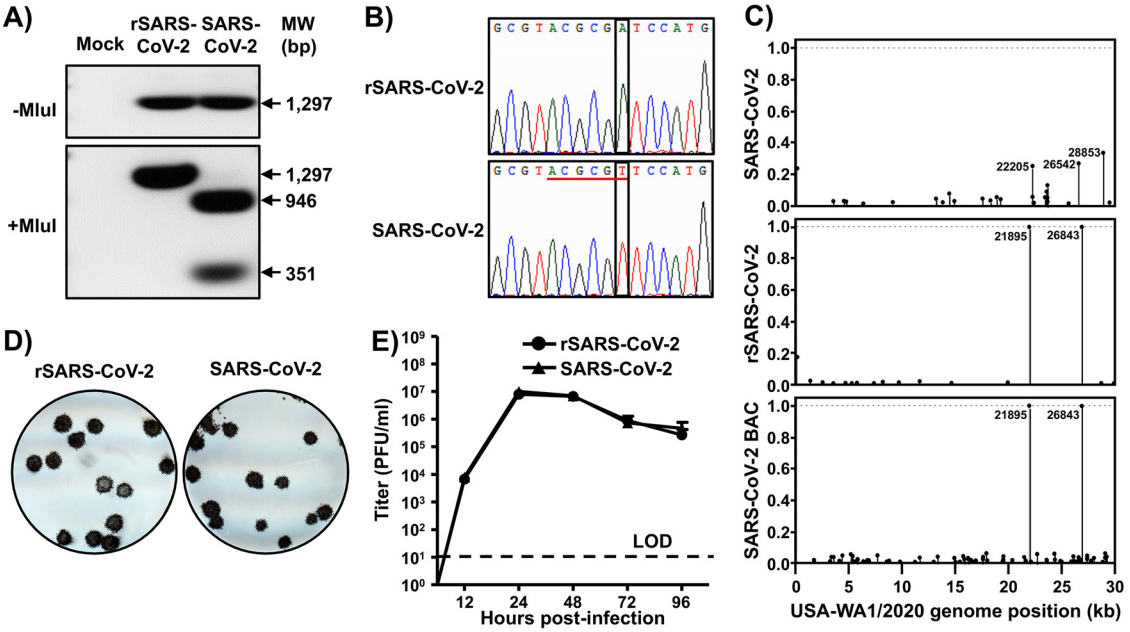

FIG 3 Characterization of rSARS2-CoV-2 *in vitro*. (A and B) Genotypic characterization. Vero E6 cells were mock infected or infected (MOI, 0.01) with rSARS-CoV-2 or the SARS-CoV-2 USA-WA1/2020 natural isolate. At 24 h postinfection, total RNA from Vero E6 cells was extracted and a 1,297-bp region of the M gene (nt 26488 to 27784) was amplified by RT-PCR. Amplified DNA was subjected to MluI digestion (Fig. 1). (A) Undigested (top) and digested (bottom) samples were separated in a 0.7% agarose gel. The RT-PCR-amplified DNA product was also sequenced to verify the presence of the silent mutation in the MluI restriction site introduced in the viral genome of the rSARS-CoV-2 (Fig. 1). (B) The MluI restriction site is underlined in red, and the silent mutation introduced to remove the MluI restriction site (T to A) is shown in the black box. (C) Verification of BAC and rSARS-CoV-2 sequences. The SARS-CoV-2 non-reference allele frequency was calculated by comparing short reads to the reference genome of the USA-WA1/2020 reference. All variants were at low frequency in the P6 natural isolate (top), the BAC (bottom), and rSARS-CoV-2 (middle), with the exception of introduced variants at positions 21895 and 26843, which were fixed in the BAC and in rSARS-CoV-2. Non-reference alleles present in less than 1% of reads are not shown. (D) Plaque phenotype. Vero E6 cells were infected with ~20 PFU of rSARS-CoV-2 (left) or the natural SARS-CoV-2 isolate (right). After 72 h of incubation at 37°C, cells were fixed and immunostained with the N protein 1C7 monoclonal antibody. (E) Growth kinetics. Vero E6 cells were infected (MOI, 0.01) with rSARS-CoV-2 or the natural SARS-CoV-2 isolate. At the indicated times postinfection, tissue culture supernatants were collected and viral titers were assessed by plaque assay (PFU/ml). Data are presented as means ± SDs. LOD, limit of detection.

replication, virulence, and pathogenicity of both SARS-CoV (23) and SARS-CoV-2 (24) *in vivo*. To confirm that the rSARS-CoV-2 RNA generated using BAC-based reverse genetics exhibited the same replication capability, virulence, and pathogenicity as the natural SARS-CoV-2 isolate *in vivo*, we infected golden Syrian hamsters intranasally with 2×10^4 PFU of either rSARS-CoV-2 or the natural SARS-CoV-2 isolate. At days 2 and 4 postinfection, we collected the nasal turbinates (upper respiratory tract) and lungs (lower respiratory tract) from infected animals, as well as mock-infected controls, to assess the gross pathological changes (lungs) and the extents of viral replication (nasal turbinates and lungs). Mild multifocal congestion and consolidation were observed in 5 to 10% of the surfaces of lungs from rSARS-CoV-2 (Fig. 4Aii)- and SARS-CoV-2 (Fig. 4Aiii)-infected animals at day 2 postinfection. As expected, the gross pathological lesions were pronounced at day 4 postinfection, with severe multifocal to locally extensive congestion and consolidation (white arrows) in 40 to 50% of the surfaces of the lungs (Fig. 4Av and vi). These lesions were widely distributed, covering both the right (cranial, medial, and caudal lobes) and the left lobes of the lungs. Particularly, the presence of frothy exudate (black arrows) in the tracheas of hamsters infected with either rSARS-CoV-2 or SARS-CoV-2 on day 4 postinfection indicates an ongoing bronchopneumonia. Of note, we did not observe significant differences in pathological lesions in the lungs at both days postinfection between animals infected with rSARS-CoV-2 or SARS-CoV-2 (Fig. 4B). Both rSARS-CoV-2 and SARS-CoV-2 replicated to similar levels in the lungs (Fig. 4C) and the nasal turbinates (Fig. 4D) of infected animals at days 2 and 4 postinfection, indicating that the genetically engineered rSARS-CoV-2 clone replicates to levels comparable to those of the natural isolate *in vivo*.

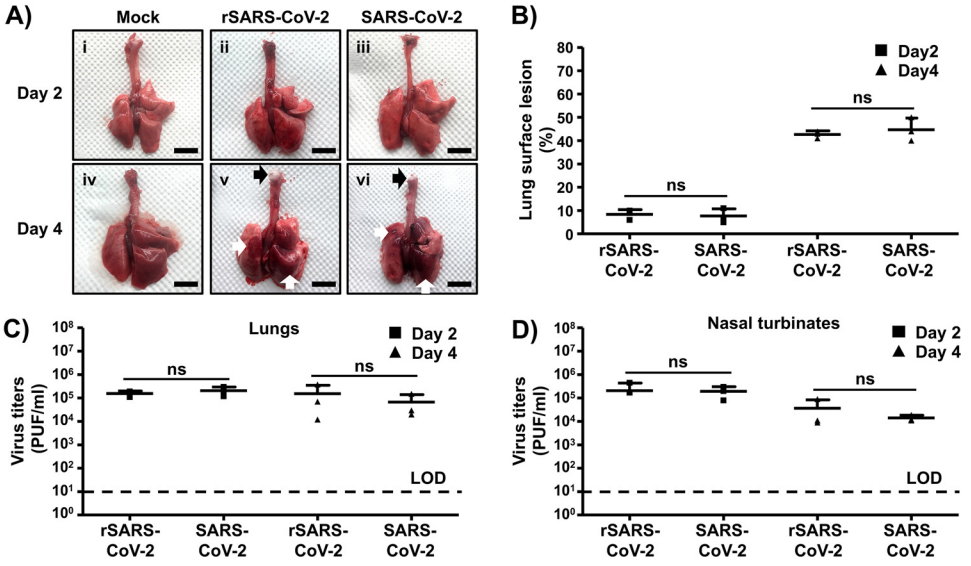

FIG 4 Pathogenicity of rescued rSARS-CoV-2 *in vivo*. Golden Syrian hamsters were mock infected ($n = 2$) or infected ($n = 6$) with 2×10^4 PFU of rSARS-CoV-2 or SARS-CoV-2. (A) Gross pathological lung lesions. Animals were euthanized at 2 and 4 days postinfection, and lungs from mock-infected (i and iv) or infected (rSARS-CoV-2 [ii and v] and SARS-CoV-2 [iii and vi]) animals were observed for gross pathological changes, including congestion and atelectasis (white arrows) and frothy trachea exudates (black arrows). Scale bars, 1 cm. (B) Macroscopic pathology scoring analysis. Distributions of pathological lesions, including consolidation, congestion, and atelectasis, were measured using ImageJ and are represented as percentages of the total lung surface area. ns, not significant. (C and D) Virus titers. Viral titers in the lungs (C) and nasal turbinates (D) of rSARS-CoV-2- and SARS-CoV-2-infected golden Syrian hamsters were determined at days 2 and 4 postinfection (3 hamsters per time point). Data are means ± SDs. ns, not significant.

DISCUSSION

The emergence of SARS-CoV-2 and associated COVID-19 disease has created an unprecedented public health threat to humans (26). To date, no FDA-approved prophylactics (vaccines) and/or therapeutics (antivirals) are available for the treatment of COVID-19, which has triggered a surge of scientific efforts to develop countermeasures to treat COVID-19 disease and control SARS-CoV-2 infection.

CoVs are single-stranded, positive-sense RNA viruses with one of the largest viral genomes (~30 kb) among RNA viruses (15). In contrast to the situation with other single-stranded RNA viruses, the development of reverse genetics systems to recover recombinant CoV has been challenging due to toxicity or the instability of viral cDNA in bacterial systems. To overcome this problem, several approaches have been used to successfully generate recombinant CoVs. This includes splitting viral cDNA for propagation in different plasmids before assembly of a full-length genome by *in vitro* ligation (27), the use of homologous recombination in yeast (28), the insertion of linker sequences that disrupt the viral open reading frame and are removed prior to transcription (29), the inactivation of cryptic promoters for bacterial RNA polymerase using silent mutagenesis (30), and the use of BACs (13–15).

Although two reverse genetics systems to generate rSARS-CoV-2 using a yeast artificial chromosome (12) or *in vitro* ligation (11) to assemble the viral genome have been described, both methods rely on *in vitro* transcription for generation of the full-length viral RNA genome and transfection of RNA into susceptible cells, a process that poses some methodological problems. In this study, we report the development of a full-length infectious clone of the SARS-CoV-2 USA-WA1/2020 strain based on the use of a BAC. This is, to our knowledge, the first reverse genetics approach to generate rSARS-CoV-2 based on the transfection of a single BAC plasmid. The full-length cDNA copy of SARS-CoV-2 USA-WA1/2020 was sequentially assembled downstream of a cytomegalovirus (CMV) promoter into the pBeloBAC11 plasmid using synthetic fragments. After delivery of the BAC into host cells, the CMV promoter initiates the

production of viral RNA from the nuclei of transfected cells by cellular RNA polymerase II. Although we described the generation of rSARS-CoV-2 from transfected Vero E6 cells, the use of the CMV promoter may also be applicable for generating rSARS-CoV-2 from other cell lines (31). Accordingly, we have been able to successfully rescue rSARS-CoV-2 using the BAC-based approach form human 293T and HeLa cells constitutively expressing human angiotensin-converting enzyme 2 (hACE2) (data not shown).

The genetic identity of the rescued rSARS-CoV-2 clone was confirmed by sequencing. Notably, the rSARS-CoV-2 clone replicated in Vero E6 cells to levels comparable to those of the natural isolate as determined by growth kinetics and plaque assay. Importantly, using the golden Syrian hamster model of SARS-CoV-2 infection (24), we found that both rSARS-CoV-2 and the natural SARS-CoV-2 isolate have similar pathogenicities and growth capabilities in the upper and lower respiratory tracts of infected animals.

In summary, we have developed, for the first time, a powerful, reliable, and convenient SARS-CoV-2 reverse genetics system based on the use of a BAC. The use of BAC-based reverse genetics for SARS-CoV-2 represents an excellent option to facilitate studies addressing a number of important concepts about the biology of SARS-CoV-2 infection. These include viral and host factors and interactions that control viral cell entry, replication, assembly, and budding, the rescue of rSARS-CoV-2 with predetermined mutations in their genomes to examine their contribution to viral multiplication and pathogenesis, the develop of cell-based approaches to interrogate individual steps in the life cycle of SARS-CoV-2 to identify the mechanism of action of viral inhibitors, the generation of rSARS-CoV-2 clones expressing reporter genes for their use in cell-based screening assays or possibly *in vivo* models for the rapid and easy identification of viral inhibitors and/or neutralizing antibodies, and the generation of rSARS-CoV-2 clones containing mutations in their viral genomes that result in attenuation for their implementation as safe, immunogenic, stable, and protective LAVs for the treatment of COVID-19 disease.

MATERIALS AND METHODS

Biosafety. All the *in vitro* and *in vivo* experiments with infectious SARS-CoV-2 were conducted under appropriate biosafety level 3 (BSL3) and animal BSL3 (ABSL3) laboratories, respectively, at the Texas Biomedical Research Institute (Texas Biomed). Experiments were approved by the Texas Biomed Institutional Biosafety Committee (IBC) and Institutional Animal Care and Use Committee (IACUC).

Cells and virus. African green monkey kidney epithelial cells (Vero E6, CRL-1586) were obtained from the American Type Culture Collection (ATCC; Bethesda, MD) and maintained in Dulbecco's modified Eagle medium (DMEM) supplemented with 5% (vol/vol) fetal bovine serum (FBS; VWR) and 100 units/ml penicillin-streptomycin (Corning).

The SARS-CoV-2 USA-WA1/2020 natural isolate was obtained from BEI Resources (NR-52281) and amplified on Vero E6 cells. This strain was selected because it was isolated from an oropharyngeal swab from a patient with respiratory illness in January 2020 in Washington, DC. The SARS-CoV-2 USA-WA1/2020 sequence was available from GenBank (accession no. MN985325).

Sequencing. We generated short-read sequencing libraries from the BAC and recovered SARS-CoV-2 viral RNA. For BAC sequencing, we followed the PCR-free KAPA HyperPlus kit protocol, using 500 ng of input RNA. For SARS-CoV-2 viral RNA sequencing, we generated libraries using a KAPA RNA HyperPrep kit with a 45-min adapter ligation incubation, including 6 cycles of PCR with 100 ng RNA and a 7 mM adapter concentration. Samples were sequenced on an Illumina HiSeq X machine.

Raw reads were quality filtered using Trimmomatic v0.39 (32) and mapped to a SARS-CoV-2 reference genome (GenBank accession no. MN985325) with Bowtie2 v2.4.1 (33). Genome coverage was quantified with MosDepth v0.2.6 (34). We genotyped each sample for low-frequency variants with LoFreq* v2.1.3.1 (35) and filtered sites with less than a 100× read depth or minor allele frequencies less than 1%. Finally, we used SnpEff v4.3t (36) to identify the impact of potential variants on the protein coding regions in the SARS-CoV-2 reference genome.

Assembly of the full length of the SARS-CoV-2 genome. Based on genomic information of the SARS-CoV-2 USA-WA1/2020 isolate deposited in GenBank (accession no. MN985325), the full-length genomic sequences were divided into 5 fragments (Fig. 1), synthesized *de novo* by Bio Basic (ON, Canada), and cloned into a high-copy-number pUC57 plasmid with designated restriction sites. A BstBI site in the S gene and an MluI site in the M gene were removed by silent mutation (Fig. 1). These mutations were introduced to ensure that these restriction sites were unique and not present in the viral genome for the assembly of the full-length SARS-CoV-2 genome and as molecular markers to distinguish the rescued rSARS-CoV-2 clone from the natural isolate (Fig. 3).

For the assembly of the entire viral genome in the BAC, fragment 1 was cloned into the pBeloBAC11 plasmid (NEB), linearized by PciI and HindIII digestion (Fig. 1). By using the preassigned restriction sites

in fragment 1, the other 4 fragments were assembled sequentially by using standard molecular biology methods (Fig. 1). All the intermediate pBeloBAC11 plasmids were transformed into commercial DH10B electrocompetent *E. coli* cells (Thermo Fisher Scientific) using an electroporator (Bio-Rad) with the conditions of 2.5 kV, 600 Ω, and 10 μF. The BAC containing the full-length SARS-CoV-2 genome, which had been analyzed by digestion using the restriction enzymes used to clone into pBeloBAC 11 (Fig. 1), was also confirmed by deep sequencing.

Rescue of rSARS-CoV-2. Virus rescue experiments were performed as previously described (19). Briefly, confluent monolayers of Vero E6 cells (10^6 cells/well, 6-well plates, triplicates) were transfected, using LPF2000, with 4.0-μg/well of the SARS-CoV-2 BAC or an empty BAC as the internal control. After 24 h, transfection medium was exchanged for postinfection medium (DMEM supplemented with 2% [vol/vol] FBS), and cells were split and seeded into T75 flasks 48 h posttransfection. After incubation for another 72 h, tissue culture supernatants were collected, labeled as P0, and stored at −80°C. The P0 virus was used to infect fresh Vero E6 cells (10^6 cells/well, 6-well plates, triplicates) (1 ml/well) for 48 h, and then cells were fixed and assessed for the presence of virus by immunofluorescence. After confirmation of the rescue, the P0 virus was subjected to 3 rounds of plaque purification and a new virus stock (P3) was made and titrated for further *in vitro* and/or *in vivo* experiments.

Immunofluorescence assay (IFA). Vero E6 cells (10^6 cells/well, 6-well plate format, triplicates) were mock infected or infected (multiplicity of infection [MOI] = 0.01) with the natural USA-WA1/2020 isolate or rSARS-CoV-2. At 48 h postinfection, cells were fixed with 10% formaldehyde solution at 4°C overnight and permeabilized using 0.5% (vol/vol) Triton X-100 in phosphate-buffered saline (PBS) for 15 min at room temperature. Cells were incubated overnight with 1 μg/ml of SARS-CoV cross-reactive N monoclonal antibody 1C7 at 4°C, washed with PBS, and stained with a fluorescein isothiocyanate (FITC)-labeled goat anti-mouse IgG (1:200). After being washed with PBS, cells were visualized and imaged under a fluorescence microscope (Olympus).

Plaque assay and immunostaining. Confluent monolayers of Vero E6 cells (10^6 cells/well, 6-well plate format, triplicates) were infected with ~20 PFU of SARS-CoV-2 USA-WA1/2020 or rSARS-CoV-2 for 1 h at 37°C. After viral adsorption, cells were overlaid with postinfection medium containing 1% low-melting-point agar and incubated at 37°C. At 72 h postinfection, cells were fixed overnight with 10% formaldehyde solution. For immunostaining, cells were permeabilized with 0.5% (vol/vol) Triton X-100 in PBS for 15 min at room temperature and immunostained using the N 1C7 monoclonal antibody (1 μg/ml) and the Vectastain ABC kit (Vector Laboratories) according to the manufacturer's instructions. After being immunostained, plates were scanned and photographed using a scanner (EPSON).

Virus growth kinetics. Confluent monolayers of Vero E6 cells (10^6 cells/well, 6-well plate format, triplicates) were infected (MOI = 0.01) with SARS-CoV-2 USA-WA1/2020 or rSARS-CoV-2. After 1 h of virus adsorption at 37°C, cells were washed with PBS and incubated in postinfection medium at 37°C. At the indicated times after infection, viral titers in tissue culture supernatants were determined by plaque assay and immunostaining using the N monoclonal antibody 1C7, as previously described (37).

RNA extraction and RT-PCR. Total RNA from SARS-CoV-2 USA-WA1/2020- or rSARS-CoV-2-infected (MOI = 0.01) Vero E6 cells (10^6 cells/well, 6-well plate format) was extracted with TRIzol reagent (Thermo Fisher Scientific) according to the manufacturer's instructions. RT-PCR amplification of the viral genome spanning nucleotides 26488 to 27784 was performed using SuperScript II reverse transcriptase (Thermo Fisher Scientific) and the Expand high-fidelity PCR system (Sigma-Aldrich). The 1,297 amplified RT-PCR products were digested with MluI (NEB). Amplified DNA products, undigested or digested with MluI, were subjected to 0.7% agarose gel analysis. Gel-purified PCR fragments were subjected to Sanger sequencing (ACGT). All primer sequences used for RT-PCR are available upon request.

Pathogenicity studies in golden Syrian hamsters. Twelve-week-old female golden Syrian hamsters were purchased from Charles River and maintained in the animal facility at Texas Biomed under specific-pathogen-free conditions. Golden Syrian hamsters were infected (1.0×10^4 PFU) intranasally with either the rSARS-CoV-2 clone or the natural USA-WA1/2020 isolate in a final volume of 100 μl following gaseous sedation in an isoflurane chamber. After viral infection, hamsters were humanely euthanized on days 2 and 4 postinfection to collect nasal turbinates and lungs.

Measurement of viral loads in nasal turbinates and lungs. Nasal turbinates and lungs from mock-, SARS-CoV-2-, and SARS-CoV-2-infected golden Syrian hamsters were homogenized in 2 ml of PBS for 20 s at 7,000 rpm using a Precellys tissue homogenizer (Bertin Instruments). Tissue homogenates were centrifuged at 12,000 × *g* (4°C) for 5 min, and supernatants were collected for the measurement of viral loads. Confluent monolayers of Vero E6 cells (96-plate format, 4×10^4 cells/well, duplicate) were infected with 10-fold serial dilutions of the supernatants from the tissue homogenates. After viral adsorption for 1 h at 37°C, cells were washed 3 times with PBS before addition of fresh postinfection medium containing 1% microcrystalline cellulose (Avicel; Sigma-Aldrich). Cells were further incubated at 37°C for 24 h. Plates were then inactivated in 10% neutral buffered formalin (Thermo Fisher Scientific) for 24 h. For immunostaining, cells were washed three times with PBS and permeabilized with 0.5% Triton X-100 for 10 min at room temperature. Then, cells were blocked with 2.5% bovine serum albumin (BSA) in PBS for 1 h at 37°C, followed by incubation with 1 μg/ml of the anti-N SARS-CoV monoclonal antibody 1C7 diluted in 1% BSA for 1 h at 37°C. After incubation with the primary antibody, cells were washed three times with PBS, counterstained with the Vectastain ABC kit, and developed using the DAB peroxidase substrate kit (Vector Laboratory, Inc., CA, USA) according to the manufacturer's instructions. Virus titers are indicated as PFU/ml.

Evaluation of lung pathological lesions. Macroscopic pathology scoring was evaluated using ImageJ software to determine the percentage of the total surface area of the lung (dorsal and ventral views) affected by consolidation, congestion, and atelectasis, as previously described (38).

Statistical analysis. Data representative of three independent experiments in triplicates have been used. All data represent the mean ± standard deviation (SD) for each group and were analyzed with SPSS13.0 (IBM). A two-tailed Student *t* test was used to compare the means between two groups. *P* values of less than 0.05 ($P < 0.05$) were considered statistically significant.

ACKNOWLEDGMENTS

We thank Thomas Moran at the Icahn School of Medicine at Mount Sinai for providing us with the SARS-CoV cross-reactive N monoclonal antibody 1C7. We also thank BEI Resources for providing the SARS-CoV-2 USA-WA1/2020 isolate (NR-52281) and Marina McDew-White and Robbie Diaz for constructing the NGS libraries. Finally, we thank members at our institutes for their efforts in keeping our facilities fully operational during the COVID-19 pandemic and the biosafety committee (BSC) and IACUC for reviewing our protocols in a time-efficient manner.

We dedicate this paper to all COVID-19 victims and to all heroes battling this disease.

REFERENCES

1. Lopez-Ortiz E, Lopez-Ortiz G, Mendiola-Pastrana IR, Mazon-Ramirez JJ, Diaz-Quinonez JA. 2020. From the handling of an outbreak by an unknown pathogen in Wuhan to the preparedness and response in the face of the emergence of Covid-19 in Mexico. Gac Med Mex 156:132–137. https://doi.org/10.24875/GMM.M20000346.
2. Ralph R, Lew J, Zeng TS, Francis M, Xue B, Roux M, Ostadgavahi AT, Rubino S, Dawe NJ, Al-Ahdal MN, Kelvin DJ, Richardson CD, Kindrachuk J, Falzarano D, Kelvin AA. 2020. 2019-nCoV (Wuhan virus), a novel Coronavirus: human-to-human transmission, travel-related cases, and vaccine readiness. J Infect Dev Ctries 14:3–17. https://doi.org/10.3855/jidc.12425.
3. Khan S, Nabi G, Han G, Siddique R, Lian S, Shi H, Bashir N, Ali A, Shereen MA. 2020. Novel coronavirus: how things are in Wuhan. Clin Microbiol Infect 26:399–400. https://doi.org/10.1016/j.cmi.2020.02.005.
4. Stoye E. 7 April 2020. The pandemic in pictures: how coronavirus is changing the world. Nature https://doi.org/10.1038/d41586-020-01048-7.
5. Qian X, Ren R, Wang YF, Guo Y, Fang J, Wu Z-D, Liu P-L, Han T-R, Members of Steering Committee, Society of Global Health, Chinese Preventive Medicine Association. 2020. Fighting against the common enemy of COVID-19: a practice of building a community with a shared future for mankind. Infect Dis Poverty 9:34. https://doi.org/10.1186/s40249-020-00650-1.
6. Vellingiri B, Jayaramayya K, Iyer M, Narayanasamy A, Govindasamy V, Giridharan B, Ganesan S, Venugopal A, Venkatesan D, Ganesan H, Rajagopalan K, Rahman PKSM, Cho SG, Kumar NS, Subramaniam MD. 2020. COVID-19: a promising cure for the global panic. Sci Total Environ 725:138277. https://doi.org/10.1016/j.scitotenv.2020.138277.
7. Jones L, Walsh K, Willcox M, Morgan P, Nichols J. 2020. The COVID-19 pandemic: important considerations for contact lens practitioners. Cont Lens Anterior Eye 43:196–203. https://doi.org/10.1016/j.clae.2020.03.012.
8. Ciotti M, Angeletti S, Minieri M, Giovannetti M, Benvenuto D, Pascarella S, Sagnelli C, Bianchi M, Bernardini S, Ciccozzi M. 2019. COVID-19 outbreak: an overview. Chemotherapy 64:215–223. https://doi.org/10.1159/000507423.
9. de Wit E, van Doremalen N, Falzarano D, Munster VJ. 2016. SARS and MERS: recent insights into emerging coronaviruses. Nat Rev Microbiol 14:523–534. https://doi.org/10.1038/nrmicro.2016.81.
10. Coutard B, Valle C, de Lamballerie X, Canard B, Seidah NG, Decroly E. 2020. The spike glycoprotein of the new coronavirus 2019-nCoV contains a furin-like cleavage site absent in CoV of the same clade. Antiviral Res 176:104742. https://doi.org/10.1016/j.antiviral.2020.104742.
11. Xie X, Muruato A, Lokugamage KG, Narayanan K, Zhang X, Zou J, Liu J, Schindewolf C, Bopp NE, Aguilar PV, Plante KS, Weaver SC, Makino S, LeDuc JW, Menachery VD, Shi PY. 2020. An infectious cDNA clone of SARS-CoV-2. Cell Host Microbe 27:841–848.e3. https://doi.org/10.1016/j.chom.2020.04.004.
12. Thao TTN, Labroussaa F, Ebert N, V'kovski P, Stalder H, Portmann J, Kelly J, Steiner S, Holwerda M, Kratzel A, Gultom M, Schmied K, Laloli L, Husser L, Wider M, Pfaender S, Hirt D, Cippa V, Crespo-Pomar S, Schroder S, Muth D, Niemeyer D, Corman VM, Muller MA, Drosten C, Dijkman R, Jores J, Thiel V. 2020. Rapid reconstruction of SARS-CoV-2 using a synthetic genomics platform. Nature 582:561–565. https://doi.org/10.1038/s41586-020-2294-9.
13. St-Jean JR, Desforges M, Almazan F, Jacomy H, Enjuanes L, Talbot PJ. 2006. Recovery of a neurovirulent human coronavirus OC43 from an infectious cDNA clone. J Virol 80:3670–3674. https://doi.org/10.1128/JVI.80.7.3670-3674.2006.
14. Almazán F, DeDiego ML, Sola I, Zuñiga S, Nieto-Torres JL, Marquez-Jurado S, Andrés G, Enjuanes L. 2013. Engineering a replication-competent, propagation-defective Middle East respiratory syndrome coronavirus as a vaccine candidate. mBio 4:e00650-13. https://doi.org/10.1128/mBio.00650-13.
15. Almazan F, Gonzalez JM, Penzes Z, Izeta A, Calvo E, Plana-Duran J, Enjuanes L. 2000. Engineering the largest RNA virus genome as an infectious bacterial artificial chromosome. Proc Natl Acad Sci U S A 97:5516–5521. https://doi.org/10.1073/pnas.97.10.5516.
16. Avila-Perez G, Nogales A, Martin V, Almazan F, Martinez-Sobrido L. 2018. Reverse genetic approaches for the generation of recombinant Zika virus. Viruses 10:597. https://doi.org/10.3390/v10110597.
17. Avila-Perez G, Nogales A, Park JG, Marquez-Jurado S, Iborra FJ, Almazan F, Martinez-Sobrido L. 2019. A natural polymorphism in Zika virus NS2A protein responsible of virulence in mice. Sci Rep 9:19968. https://doi.org/10.1038/s41598-019-56291-4.
18. Avila-Perez G, Nogales A, Park JG, Vasquez DM, Dean DA, Barravecchia M, Perez DR, Almazan F, Martinez-Sobrido L. 2020. In vivo rescue of recombinant Zika virus from an infectious cDNA clone and its implications in vaccine development. Sci Rep 10:512. https://doi.org/10.1038/s41598-020-57545-2.
19. Ávila-Pérez G, Park J-G, Nogales A, Almazán F, Martínez-Sobrido L. 2019. Rescue of recombinant Zika virus from a bacterial artificial chromosome cDNA clone. J Vis Exp 148:e59537. https://doi.org/10.3791/59537.
20. Marquez-Jurado S, Nogales A, Avila-Perez G, Iborra FJ, Martinez-Sobrido L, Almazan F. 2018. An alanine-to-valine substitution in the residue 175 of Zika virus NS2A protein affects viral RNA synthesis and attenuates the virus in vivo. Viruses 10:547. https://doi.org/10.3390/v10100547.
21. Martinez-Sobrido L, Almazan F. 2019. New advances on Zika virus research. Viruses 11:258. https://doi.org/10.3390/v11030258.
22. Cheng BY, Ortiz-Riano E, de la Torre JC, Martinez-Sobrido L. 2013. Generation of recombinant arenavirus for vaccine development in FDA-approved Vero cells. J Vis Exp 78:e50662. https://doi.org/10.3791/50662.
23. Roberts A, Vogel L, Guarner J, Hayes N, Murphy B, Zaki S, Subbarao K. 2005. Severe acute respiratory syndrome coronavirus infection of golden Syrian hamsters. J Virol 79:503–511. https://doi.org/10.1128/JVI.79.1.503-511.2005.
24. Sia SF, Yan L-M, Chin AWH, Fung K, Choy K-T, Wong AYL, Kaewpreedee P, Perera RAPM, Poon LLM, Nicholls JM, Peiris M, Yen H-L. 2020. Pathogenesis and transmission of SARS-CoV-2 in golden hamsters. Nature 583:834–838. https://doi.org/10.1038/s41586-020-2342-5.
25. Ye C, de la Torre JC, Martinez-Sobrido L. 2020. Reverse genetics approaches for the development of mammarenavirus live-attenuated vaccines. Curr Opin Virol 44:66–72. https://doi.org/10.1016/j.coviro.2020.06.011.
26. Sohrabi C, Alsafi Z, O'Neill N, Khan M, Kerwan A, Al-Jabir A, Iosifidis C, Agha R. 2020. World Health Organization declares global emergency: a review of the 2019 novel coronavirus (COVID-19). Int J Surg 76:71–76. https://doi.org/10.1016/j.ijsu.2020.02.034.

27. Sumiyoshi H, Hoke CH, Trent DW. 1992. Infectious Japanese encephalitis virus RNA can be synthesized from in vitro-ligated cDNA templates. J Virol 66:5425–5431. https://doi.org/10.1128/JVI.66.9.5425-5431.1992.
28. Polo S, Ketner G, Levis R, Falgout B. 1997. Infectious RNA transcripts from full-length dengue virus type 2 cDNA clones made in yeast. J Virol 71:5366–5374. https://doi.org/10.1128/JVI.71.7.5366-5374.1997.
29. Tsetsarkin KA, Kenney H, Chen R, Liu G, Manukyan H, Whitehead SS, Laassri M, Chumakov K, Pletnev AG. 2016. A full-length infectious cDNA clone of Zika Virus from the 2015 epidemic in Brazil as a genetic platform for studies of virus-host interactions and vaccine development. mBio 7:e01114-16. https://doi.org/10.1128/mBio.01114-16.
30. Pu SY, Wu RH, Yang CC, Jao TM, Tsai MH, Wang JC, Lin HM, Chao YS, Yueh A. 2011. Successful propagation of flavivirus infectious cDNAs by a novel method to reduce the cryptic bacterial promoter activity of virus genomes. J Virol 85:2927–2941. https://doi.org/10.1128/JVI.01986-10.
31. Qin JY, Zhang L, Clift KL, Hulur I, Xiang AP, Ren B-Z, Lahn BT. 2010. Systematic comparison of constitutive promoters and the doxycycline-inducible promoter. PLoS One 5:e10611. https://doi.org/10.1371/journal.pone.0010611.
32. Bolger AM, Lohse M, Usadel B. 2014. Trimmomatic: a flexible trimmer for Illumina sequence data. Bioinformatics 30:2114–2120. https://doi.org/10.1093/bioinformatics/btu170.
33. Langmead B, Salzberg SL. 2012. Fast gapped-read alignment with Bowtie 2. Nat Methods 9:357–359. https://doi.org/10.1038/nmeth.1923.
34. Pedersen BS, Quinlan AR. 2018. Mosdepth: quick coverage calculation for genomes and exomes. Bioinformatics 34:867–868. https://doi.org/10.1093/bioinformatics/btx699.
35. Wilm A, Aw PP, Bertrand D, Yeo GH, Ong SH, Wong CH, Khor CC, Petric R, Hibberd ML, Nagarajan N. 2012. LoFreq: a sequence-quality aware, ultra-sensitive variant caller for uncovering cell-population heterogeneity from high-throughput sequencing datasets. Nucleic Acids Res 40:11189–11201. https://doi.org/10.1093/nar/gks918.
36. Cingolani P, Platts A, Wang Le L, Coon M, Nguyen T, Wang L, Land SJ, Lu X, Ruden DM. 2012. A program for annotating and predicting the effects of single nucleotide polymorphisms, SnpEff: SNPs in the genome of Drosophila melanogaster strain w1118; iso-2; iso-3. Fly (Austin) 6:80–92. https://doi.org/10.4161/fly.19695.
37. Nogales A, Baker SF, Ortiz-Riano E, Dewhurst S, Topham DJ, Martinez-Sobrido L. 2014. Influenza A virus attenuation by codon deoptimization of the NS gene for vaccine development. J Virol 88:10525–10540. https://doi.org/10.1128/JVI.01565-14.
38. Jensen EC. 2013. Quantitative analysis of histological staining and fluorescence using ImageJ. Anat Rec (Hoboken) 296:378–381. https://doi.org/10.1002/ar.22641.